Plasma Sources Science and Technology

PAPER

A model for etching of three-dimensional high aspect ratio silicon structures in pulsed inductively coupled plasmas

To cite this article: J-C Wang *et al* 2018 *Plasma Sources Sci. Technol.* **27** 094003

Plasma Sources Sci. Technol. **27** (2018) 094003 (17pp)

https://doi.org/10.1088/1361-6595/aadb4b

A model for etching of three-dimensional high aspect ratio silicon structures in pulsed inductively coupled plasmas

J-C Wang[1], W Tian[1], S Rauf[1], S Sadighi[1], J Kenney[1], P Stout[1], V S Vidyarthi[1], J Guo[1], T Zhou[1], K Delfin[1], N Lundy[1], S C Pandey[2], S Guo[2] and G S Sandhu[2]

[1] Applied Materials, Inc., 1140 E. Arques Ave., Sunnyvale, CA 94085, United States of America

[2] Micron Technology, Inc., 8000 S. Federal Way, Boise, ID 83707, United States of America

E-mail: shahid_rauf@amat.com

Received 3 April 2018, revised 23 July 2018
Accepted for publication 20 August 2018
Published 14 September 2018

Abstract

A coupled plasma—feature scale model is employed to investigate the etching of high aspect ratio (HAR) silicon (Si) structures using a cyclic multi-step pulsed plasma process in an inductively coupled plasma (ICP) reactor. This process sequence includes an oxidation step to help protect the Si sidewalls, a main Si etch step where the ion energy and angular distribution (IEAD) and ion/neutral flux ratio are controlled through power pulsing, and a clean step prior to repeating the multi-step process. Two-dimensional plasma models are used to compute the IEAD as well as the fluxes of relevant ions and neutral radicals at the wafer. These plasma models are coupled to a three-dimensional feature scale model, where multiple cycles of the three-step etch sequence are simulated. The paper focuses on evaluation of several pulsing modes during the main Si etch step including separate pulsing of the ICP source or RF bias power, and their synchronized pulsing (with phase control). Process performance has been quantitatively evaluated by examining etch rates for Si and the SiO_2-like mask, Si/mask etch selectivity, and CDs within the HAR features. When only the RF bias power is pulsed, Si and mask etch rates scale with pulse duty cycle (DC). As a result, if Si is etched to the same depth, the HAR trenches are wider at higher DCs due to less total oxidation time and less protection of the sidewalls. ICP source power pulsing provides higher Si etch rate because of RF bias power being on continuously, but suffers from poor mask selectivity. Synchronized pulsing of both the ICP source and RF bias powers in conjunction with phase control provides additional flexibility in modulating the IEAD and the ion/neutral flux ratio. RF bias pulsing and in-phase synchronized pulsing yield the best selectivity for the conditions explored.

Keywords: plasma etching, plasma modeling, feature scale modeling, Si etching, shallow trench isolation, pulsed plasma

1. Introduction

Most microelectronic technologies are based on silicon (Si), and Si etching is a well-established manufacturing process [1]. However, as device critical dimensions (CDs) shrink below 10 nm, Si etching is experiencing multiple challenges. One can examine some of these challenges in the context of shallow trench isolation (STI), which has replaced local oxidation of silicon and become a key process in today's integrated circuits [2]. One of the important steps during STI formation is etching a pattern of trenches in Si. The width of these trenches can vary from 100 nm to sub-10 nm in advanced microelectronic devices, with depths varying from 200 to 600 nm. It is challenging to etch such high aspect ratio (HAR) features with final structures having low sidewall roughness, desirable profile, and minimal aspect ratio dependence. Wu *et al* [3] reviewed the challenges of HAR Si etch, explaining that optimum performance strongly relies on enhancing the vertical etch rate while reducing the lateral etch rate. The incident ion energy and angle distribution (IEAD) and passivation on the sidewalls were found to be critical for the etch process.

To meet the challenges of sub-10 nm device fabrication, Si etching has undergone many changes in recent years. HAR etching generally requires ions with high energy, which reduces their angular spread. The presence of high energy ions turns the mask into a critical factor for etch process design. Photolithography process margin requirements have led to thinner photo-resists (PRs), which reduces the etch process margin making it necessary to use harder masks. SiO_2 has gradually replaced PR as the preferred mask for etching of small Si structures. Cho *et al* [4] investigated the patterning process using SiO_2 hard-mask and found that the hard-mask improved the trench profile and provided a wider margin for etching. Traditional PR mask resulted in collapsed scallop patterns with smaller CDs. Choi and Hong [5] compared the etching results with PR and SiO_2 masks during fabrication of small structures. They found that SiO_2 hard mask provided better Si etch rate and smoother sidewalls compared to the PR mask.

The plasma used for the etching process is critical since it provides energetic ions and chemically reactive radicals. Power-modulated (pulsed) plasmas have demonstrated several advantages compared to continuous wave (CW) plasmas and have become indispensable in etching of the next generation of microelectronic devices with characteristic dimensions below 10 nm [6]. Specifically, pulsed plasmas can result in better uniformity, and generate less structural, electrical, or radiation (e.g. vacuum ultraviolet) induced damage [7]. Pulsed plasmas have also been demonstrated to ameliorate unwanted artefacts during etching such as notching, bowing, micro-trenching, and aspect ratio dependent etching [8]. Additionally, pulsed plasmas can be used to control the ion energy and produce narrow ion angular distributions, which is important for HAR etching [9].

Due to stringent etching requirements for sub-10 nm devices, it has become necessary to decouple sidewall passivation and Si etching. Such decoupling had been done previously for deep Si etching using the Bosch etch process [10]. Passivation helps protect the Si sidewalls and allows one to etch deeper with minimal lateral etching. The bottom surface of the feature is fully bombarded by incident ions while the passivation layer protects the sidewalls. Since excessive passivation or polymerization can dramatically reduce the etch rate and lead to etch stop, careful balance between etch and passivation processes is critical for HAR etching. Additional cleaning steps can be used to remove etch residues, which can interfere with subsequent passivation. O_2 is an attractive passivation gas during Si etching. Dussart *et al* [11] experimentally investigated the passivation mechanism in SF_6/O_2 etching process and found that O atoms are necessary for the formation of the passivation layer. Blauw *et al* [12] modeled the effect of oxygen sidewall passivation in fluorine-based anisotropic plasma etching of silicon trenches. Their simulations highlighted the importance of fluorine-to-oxygen ratio to oxygen passivation formation. Azimi *et al* [13] separated the $H_2/O_2/SF_6$ based passivation process from the etch process. This multistep process enabled better control of the growth of the passivation layer and the passivation and etch processes could be independently tuned to achieve the desired characteristics.

With the increasing complexity of cyclic processing and the large number of process variables, three-dimensional (3D) feature scale modeling becomes attractive as it can provide keen insights into the fundamental etching and deposition mechanisms [14, 15]. For example, during the multi-step etching process, usually consisting of passivation and etching steps, the model can investigate the effect of individual steps on the final results. Rauf *et al* [16] used a two-dimensional (2D) feature scale model to investigate a multi-step deep Si etch process involving alternative etching and sidewall passivation steps. They developed the surface reaction mechanism using experimental data. Their feature scale model showed details of the dynamics of multi-step deep Si etching and how the etching characteristics could be controlled by varying gas pressure, bias power, and relative step times. Coupling plasma reactor and feature scale models is important as it provides insight into the connection between the control variables and final processing results. For example, the non-uniformity of the plasma across the wafer causes differences in the local evolution of the feature profiles. Hoang *et al* [17] developed a Monte Carlo feature scale model for STI Si etch in chlorine-based plasmas. They used the plasma species ratios from a reactor scale model as input for the feature scale model. The feature scale model was calibrated using carefully designed experiments and used to investigate etching variation from the center to the edge of the wafer. Their modeling results accurately captured processing details such as sidewall bowing, micro-trenching, and faceting.

This article focuses on a coupled 2D plasma—3D feature scale model for HAR Si etching. The model is applied to a cyclic multi-step etch process in which the inductively coupled plasma (ICP) source and radio-frequency (RF) bias powers are pulsed during the main Si etch step. Processing results are examined for several pulsing modes including RF bias pulsing, ICP source power pulsing, and synchronized source and bias pulsing.

The remainder of this article is organized as follows. Our computational model is described in section 2. Section 3 contains the primary modeling results. The article concludes with a summary in section 4.

2. Computational model

Plasma simulations in this article use CRTRS [18, 19], a one/two/three-dimensional hybrid plasma model. This model includes Poisson's equation, continuity equations for all charged and neutral species, drift-diffusion approximation for electron flux, momentum conservation equation for positive ions, and the electron energy conservation equation. During the computation, at every time step, the coupled set of Poisson's equation, continuity equations for charged species, and the ion momentum equations are first solved implicitly. This is followed by implicit solution of the electron energy conservation equation and explicit solution of neutral continuity equations. The plasma transport model is coupled to an electromagnetic model for computing the inductive electric field and power deposition. Computational methodology for the electromagnetic model and its coupling to the plasma transport model are like those described by Ventzek *et al* [20].

The plasma model includes the ability to impose arbitrary pulsed power schemes for both inductive- and capacitive-coupled sources. At a basic level, this allows control of pulse frequencies, duty cycles (DCs), and phases for specified sources. In addition, temporally and spatially resolved density and electric field data are captured periodically for use in a coupled Monte Carlo particle simulation. This particle simulation generates IEADs, which vary during the pulse depending on its characteristics.

The feature scale model used is Papaya [21]. Papaya is a lattice Monte Carlo model, which resolves the surface materials of the wafer using a 3D lattice mesh. The surface is defined as the boundary between occupied and unoccupied lattice cells. Each numerical lattice cell represents a solid material, such as Si or SiO_2. The fluxes of reactant species and their energy and angular distributions are obtained from the plasma model. The reactor to feature coupling is one-way. The species are injected as pseudo-particles at the source plane in the feature model based on the rates, angles and energies calculated in the reactor model. Lagrangian particle tracking is used to transport specie from the source plane to the feature surface. At a few Pa pressure, an assumption is made that no gas-gas collisions will occur during the species approach from source plane to the feature surface since the mean-free-path of the incoming specie is much larger than the feature size. When a pseudo-particle strikes the surface, reactions including reflection, deposition, etching and sputtering can occur depending on a probability matrix. This probability matrix is determined by the incident fluxes, IEAD, and the surface reaction mechanism.

In order to bridge the disparate timescales among the RF cycle ($\sim 10^{-6}$ s), pulse duration ($\sim 10^{-3}$ s), and etching time ($\sim 10^{1}$ s) for a pulsed process, species fluxes and energies calculated at different stages of the pulse are averaged for use in the feature scale model using the following scheme: during each pulse period, 50 equally-spaced snapshots are taken of fluxes Γ_i^n (at time n for species i) and ion energy and angular distributions IEAD_i^n. Pulse-averaged fluxes for each species are calculated using a straight average of the flux snapshots. A composite IEAD is then generated for each ion species using the individual snapshots, weighted by the corresponding ion flux for that snapshot. The forms of these calculations are shown in equations (1) and (2), respectively:

$$\overline{\Gamma_i} = \sum_{n=1}^{50} \Gamma_i^n / 50, \tag{1}$$

$$\overline{\mathrm{IEAD}_i} = \sum_{n=1}^{50} (\Gamma_i^n \cdot \mathrm{IEAD}_i^n) \Big/ \sum_{n=1}^{50} \Gamma_i^n. \tag{2}$$

Table 1. Species considered in the surface reaction mechanism.

Process step	Species
Oxidation	Ar^+, O^+, O_2^+ and O
Si etch	Cl_2^+, Cl^+, Br^+, HBr^+, H^+, Cl, Br and BP (Byproducts)
Clean	Ar^+, CF_x^+ ($x = 1 - 3$), CF_x ($x = 1 - 3$) and F

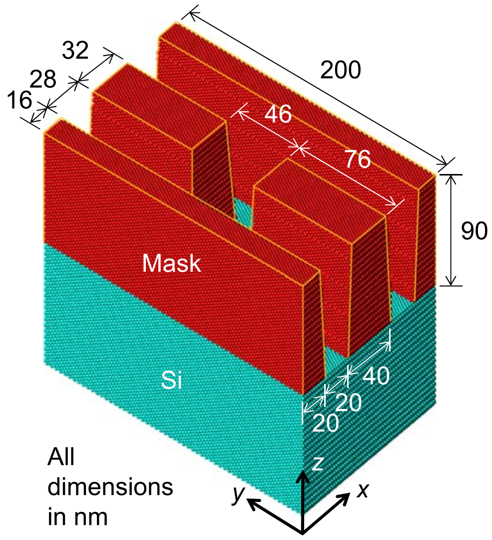

Figure 1. Initial structure used for feature profile simulations.

We have based the surface reaction mechanism in the feature profile simulation on previous studies in the literature on Si and SiO_2 etching in relevant chemistries [22–25]. Reaction rates, sticking coefficients and yields for these processes have, however, been empirically estimated through comparison with experiments. As this experimental data is proprietary and unpublished, we only describe the general framework of our surface reaction mechanism below. The primary species in this surface reaction are shown in table 1. All major reactive radicals and ions in the plasma model are considered but some have been lumped together for convenience (e.g., Br and Br^*, Cl and Cl^*). As charging is not considered in this work, the negatively charged species such as electrons and F^- are ignored. Our Si etch plasma model currently does not self-consistently include etch byproducts (e.g., $SiCl_x$, $SiBr_y$). The byproducts (BP) have been directly introduced in the feature scale model and their flux is assumed to be proportional to the RF bias DC. The material stack we use in the feature scale model is shown in figure 1. It consists of crystalline Si and SiO_2-like mask. The mask material has been deposited using plasma enhanced chemical vapor deposition with Tetraethyl orthosilicate (TEOS) precursor in a capacitively coupled plasma reactor and is amorphous [26]. Mask's pertinent etch properties (etch yield versus ion energy, angular dependence of yield) have been estimated through comparison with unreported experimental measurements.

The surface reaction mechanism in the feature scale model is shown in table 2. We model multiple cycles of a three-step process sequence: oxidation, main Si etching, and

Table 2. Reaction mechanism for the multi-step Si etching process.

No.	Process	Reactions[a]
1	Si oxidation	$O + Si(s) \rightarrow SiO_x(s)$
2	Si passivation/activation	$Cl/Br + Si(s) \rightarrow Si^*(s)$
3	Si reactive ion etch	$Ion + Si^*(s) \rightarrow Gas$
4	Si sputtering	$Ion + Si(s) \rightarrow Gas$
5	Si chemical etch	$F + Si(s)/Si^*(s) \rightarrow Gas$
6	Polymerization/activation on mask	$CF_x + TEOS(s) \rightarrow SiO_x{}^*(s)$
7	Polymerization/activation on SiO	$CF_x + SiO_x(s) \rightarrow SiO_x^*(s)$
8	Reactive ion etch of SiO_x	$Ion + SiO_x^*(s) \rightarrow Gas$
9	Sputtering of mask	$Ion + TEOS(s) \rightarrow Gas$
10	Sputtering of SiO_x	$Ion + SiO_x(s) \rightarrow Gas$
11	Byproduct redeposition	$BP + Material(s) \rightarrow Si(s) + Material(s)$

[a] Glossary: $SiO_x(s)$—Oxidized Si. TEOS(s)—SiO_2-like material deposited using TEOS precursor. $Si^*(s)$—Si(s) with Cl and Br passivation. Gas—Etch effluent, which is not further considered in the model. $SiO_x{}^*(s)$—$SiO_x(s)$ with CF_x polymer/passivation layer. BP—Etch byproducts. Material(s)—Any material.

clean. During the oxidation step, Ar^+, $O_2{}^+$, O^+, and O are generated in the plasma. The energy of the ions is low because no RF bias power is applied. In our mechanism, we do not account for the ions in the oxidation step as the neutral O flux is larger than ion fluxes by a factor of 10^3. O oxidizes Si near its surface producing SiO_x. During the Si etch step, primary ions include $Cl_2{}^+$, Cl^+, Br^+, HBr^+, and H^+, and reactive neutrals include Cl and Br. Although negative ions (Cl^-, Br^-) could potentially reach the wafer when both ICP source and RF bias powers are off during pulsing, the plasma potential has collapsed then and negative ion energy is negligible. We have therefore not considered negative ions in the Si etch mechanism. The etching mechanism includes passivation of Si by Cl and Br, physical sputtering of Si, and reactive ion etch of the passivated Si. The ion energy, which can be greater than 1000 eV, is sufficient for sputtering of both Si and the TEOS mask. Our mechanism includes Si byproduct redeposition and it is assumed that redeposited material acts like pristine Si. During the clean step, $CF_x{}^+$ ($x = 1 - 3$) ions, Ar^+, CF_x ($x = 1 - 3$) radicals, and F are generated in the plasma. The TEOS mask or SiO_x can be reactive ion etched through a combination of CF_x radicals and ions. The mechanism also includes sputtering of TEOS and SiO_x, and F chemical etching of Si. We have neglected charging due to electrons, positive ions and negative ions in the feature scale model . Even though the mask is a dielectric material, it is coated with redeposited Si containing byproducts and $SiO_xC_yF_z$ during the etch process, which can be partially conductive [27]. This model has been extensively compared to experimental data (unreported due to proprietary nature of this data) and modeling results reasonably match experimental observations. We have not observed any artefacts (e.g., line bending, notching) in the experiments that would indicate that charging is playing a role.

Etching has been done using the three-step sequence shown in table 3. These steps are repeated multiple times until the desired depth is achieved. Source and bias powers are pulsed during the main Si etch step. For all simulations reported in this article, the pulse ramp-on and ramp-off times are 1% of the pulse period, and these ramp periods are included in the specified DC. All pulsing is done at 2 kHz. Table 3 mentions the references where plasma chemistry mechanisms for the different steps (Ar/O_2, HBr/Cl_2, Ar/CF_4) are described. Plasma sources in these references are different from our ICP plasma, so details of plasma dynamics in these papers do not apply here.

3. Computational results

In this article, we examine etching of the 3D structure shown in figure 1 using multiple cycles of the three-step process sequence in table 3. This structure includes some of the critical topographic features encountered during STI etching in microelectronic device fabrication. The mask is a SiO_2-like thin film that has been deposited using plasma enhanced chemical vapor deposition with TEOS precursor. The underlying material is crystalline Si. The sidewalls of the 90 nm thick mask are assumed to be tapered at an angle of 87.455° [$=\tan^{-1}$ (90/4)]. We intend to etch Si to a depth of 400 nm and keep the Si sidewalls as vertical as possible. With such a HAR (=height/width) in the trenches, even small flux of ions on the sidewalls can lead to significant lateral etching, increasing the trench width (i.e., CD). Therefore, following current industry practices, we consider etching using the three-step process sequence in table 3. These steps are repeated multiple times, referred to as cycles in this article, until one has etched to the desired depth. The three-step cycle starts with oxidation using an O_2 ICP without RF bias. ICP source power is kept continuously on during the oxidation step. This step is expected to oxidize the exposed Si surfaces, especially the sidewalls. The second step is main Si etch, which utilizes HBr/Cl_2 plasma with RF bias. Both ICP source and RF bias powers can be pulsed during this step, and we explore several pulsing schemes in this article. Following Si etching, an Ar/CF_4 plasma with low RF bias power is used to clean residues from the surfaces. Both ICP and RF bias power are kept continuously on during the clean step.

To help interpret later feature scale simulation results, we first discuss characteristics of the oxidation and clean plasmas. All plasma simulations have been done for the ICP reactor shown in figure 2(a). This reactor has stacked ICP coils above a dielectric lid. A center nozzle introduces gas flow, which exits in the annular space at the reactor bottom. RF bias power at 2 MHz is applied to the bottom electrode, and the wafer is placed on the top of this bottom electrode.

In figure 2, we consider the inductively-coupled only oxidation process. Plasma is generated by CW ICP source power at 1500 W and no bias power is applied during the oxidation process. For this 100/100 Ar/O_2 mixture, Ar^+ is the dominant ion, as shown in figure 2(a). Here, the ion density peaks near the reactor center owing to diffusion and

Table 3. The three-step etch process.

Process	Pressure (Pa)	RF power (W)	Bias power (W)	Chemistry	Gas flow rate (sccm)	Time (s)	References
Oxidation	2	1500	0	Ar/O_2	100/100	14	[28]
Si etch	2	500	200	HBr/Cl_2	200/100	11.2	[29]
Clean	2	500	25	Ar/CF_4	100/100	4	[28]

quenching at the reactor surfaces at this relatively low pressure. A similar profile develops for O_2^+ owing to the same ion dynamics, albeit at a peak of ~20% of the Ar^+ level, as shown in figure 2(b). Finally, the O radical profile is shown in figure 2(c). This also peaks near the reactor center but sees smaller variation throughout the reactor, as it is not influenced by drift and experiences smaller surface losses (through recombination). Since oxidation of Si is primarily due to O radicals, a uniform O density over the wafer is preferable.

The clean process shares many characteristics with the oxidation process and is examined in figure 3. The plasma is generated by CW ICP source power at 500 W, and the bottom electrode is biased with 25 W during the clean process. For this 100/100 Ar/CF_4 mixture, Ar^+ is the dominant ion and, through a similar combination of drift and wall losses, peaks near the reactor center with profile as shown in figure 3(a). The small amount of RF bias power applied in this process does not significantly perturb the plasma density near the wafer. One relevant radical for residue removal, CF_3, is depicted in figure 3(b). This species shows relatively small variations across the reactor with the same dynamics as the O radicals from the oxidation step. The small RF bias power imparts a moderate Ar^+ ion energy, as shown by the Monte Carlo particle simulation result in figure 4. The bimodal distribution is typical for the application of a single low-frequency sinusoidal waveform.

Focusing on the main Si etch step, we first consider the baseline Si etch process with CW ICP source power at 500 W and pulsed RF bias power at 200 W. The RF bias power is pulsed at 2 kHz pulse frequency with 20% DC. The computed RF bias power is shown in figure 5. Here one can observe the characteristic delay in reaching peak power at the onset of the pulse owing to the ramp rate (1% of pulse period) and conservative power controller settings employed, which limit the increase in applied voltage to prevent overshooting the target. The RF bias power, however, does not have a large impact on bulk plasma quantities as the source power dominates plasma production and its characteristics. This can be seen in figures 6 and 7, where the Cl_2^+ (dominant ion) and Cl radical densities, respectively, are plotted at different stages of the RF bias pulse. For the Cl_2^+ ions, the profile just before the RF bias power is turned off (19% pulse period) is remarkably similar to that just before the RF bias power is turned back on (100% pulse period). Differences are limited to the region immediately above the cathode, where application of RF bias power results in sheath expansion and a reduction in plasma density. For Cl radicals, profiles at these same stages of the pulse are virtually indistinguishable, as bias power contributes little to their production, and they are not subject to drift. Ion energies and fluxes to the wafer are significantly impacted by the pulsing of the bias power, as shown in figure 8. Ion energy distributions for Cl_2^+ during different stages of the bias pulse show significant variation. While the bias power ramps up (4%) and down (20%), ion energies are somewhat lower than their peak when the pulse is fully established (8% and 18%). Fairly quickly after the bias power is turned off (24%), energies plummet to a unimodal distribution with low energy characteristic of an ICP-only discharge. In figure 8(b), the variation in ion fluxes during the pulse for the major ion species is given. Profiles have some common features: An initial increase in ion flux as the bias is turned on and the thicker sheath is established, which slowly decays while the power is on. Then, the ion flux drops significantly when the RF bias power is turned off and the sheath at the wafer contracts, slowly increasing toward a steady-state.

Ion and neutral species fluxes and IEAD from the above plasma simulations were coupled to the 3D feature scale model. We next examine the feature scale results for the baseline case of bias pulsing with 20% DC. We have plotted the 2D xz profile of the structure (viewed from the $y < 0$ region) in figure 9 as we progress through the etching process. Under these conditions, more than 400 nm of Si etches after 15 cycles of the three-step sequence. The mask has undergone considerable erosion during the etch process and the top corners have been rounded. The resulting larger mask opening starts to impact the top of the Si lines by the end of the etch process. The Si sidewalls are slightly tapered (0.58° from normal after 15 cycles). The tapered sidewalls in the mask certainly contribute to Si sidewall tapering, but oxidation of the Si sidewall during the oxidation step also plays a major role. Si is primarily etched through reactive ion etching by a combination of Cl, Br and energetic ions in our etch mechanism. The ion flux at the bottom Si surface is uniform due to high ion energy and the concomitant narrow ion angular distribution. However, flux of neutral species is sensitive to the view factor (i.e., how much of the plasma is visible from a given location on the surface), and all regions on the Si surface do not etch identically. To visualize the 3D structure after etching, we have shown several 2D cross-sections in figure 10 after 14 cycles. Figure 10(a) contains the xz profile of the structure as viewed from the $y < 0$ region. Figure 10(b) includes a thin xz slice around $y = 100$ nm, and figure 10(c) is the yz profile of a thin slice around $x = 60$ nm. One can observe that when the opening is wider, the sidewalls in figures 10(b) and (c) are more vertical. The effective aspect ratio is smaller for wider openings, which results in less shadowing of the neutral etchants at the feature bottom. It is clear from figure 10(b) that the bottom Si surface is not

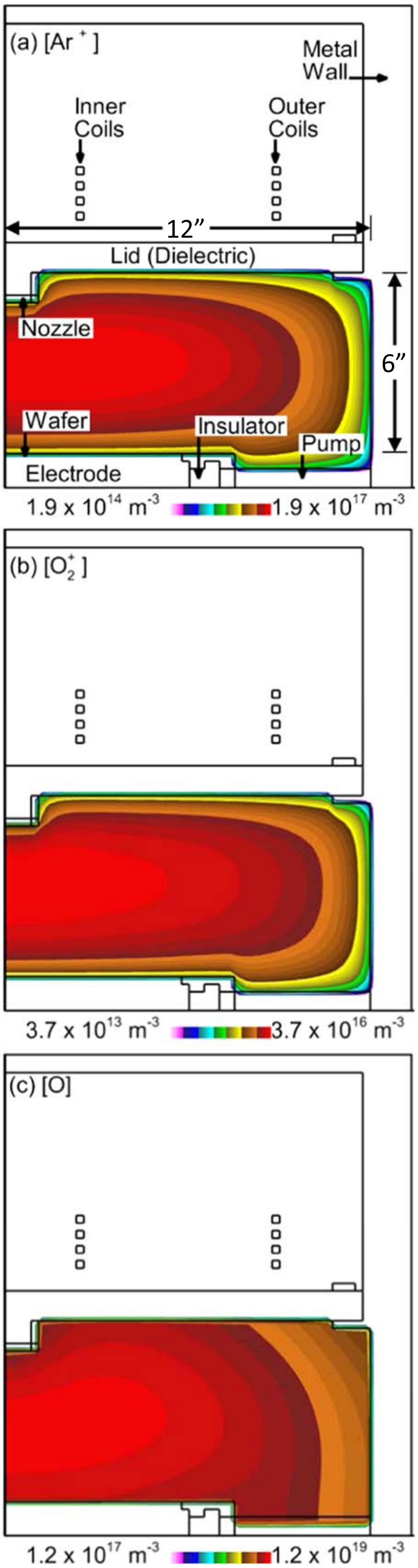

Figure 2. Species densities for the oxidation process: (a) Ar^+, (b) $O_2{}^+$, and (c) O radical. Process conditions are 2 Pa gas pressure, $Ar/O_2 = 100/100$ sccm gas flow, and 1500 W ICP source power. Plasma peaks near the reactor center primarily due to diffusion at relatively low pressure and loss to the chamber wall.

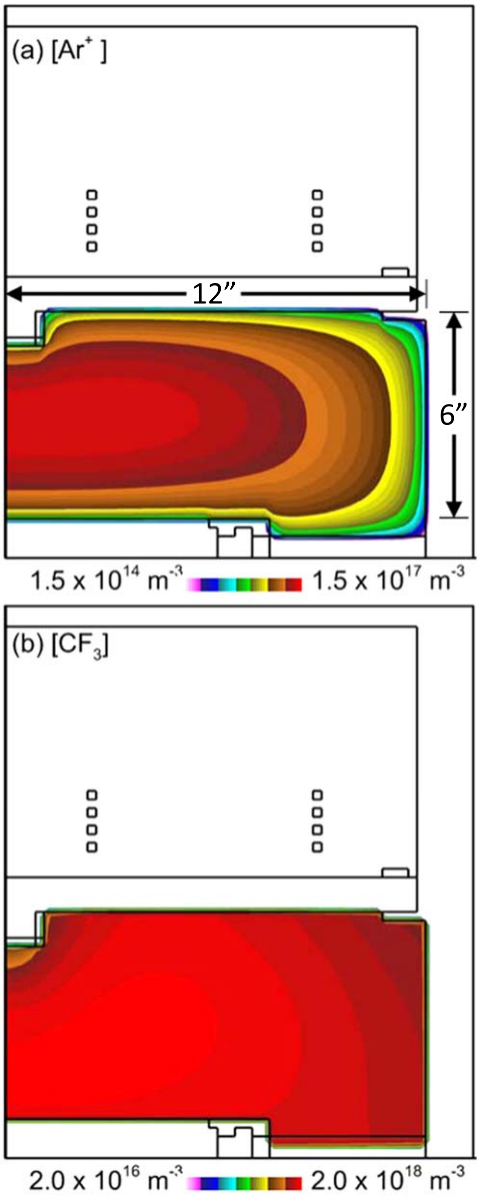

Figure 3. Species densities for the clean process: (a) Ar^+ and (b) CF_3 radical. Process conditions are 2 Pa gas pressure, $Ar/CF_4 = 100/100$ sccm gas flow, 500 W ICP source power, and 25 W RF bias power at 2 MHz.

planar. To explain the Si etch rate variation at the bottom Si surface, we have plotted the structure after 14 etch cycles in figure 11. All material above $z = -400$ nm has been removed in this plot. Also, Si macro-particles have been colored based on their z location. It can be observed that Si has etched fastest where the bottom surface is visible from both directions. In the center of the interline region, the etch depth is commensurate with the Si etch depth along the narrow trenches. Even though there is more neutral etchant flux in the inter-line region, the byproduct and O fluxes are also larger, and the two effects appear to cancel each other out for our conditions.

It is important to quantitatively examine the processing results from our 3D feature scale simulation. In figure 12, we have plotted the etch rate/cycle at the bottom of the trenches,

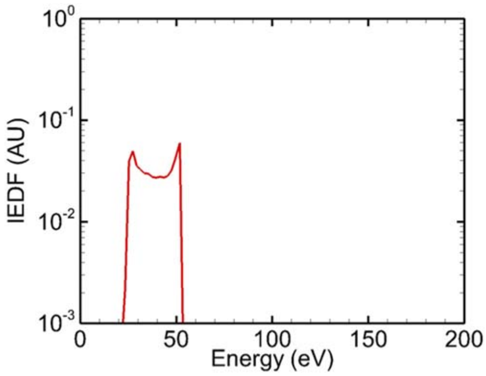

Figure 4. Ar^+ ion energy distribution function for the clean process. Process conditions are 2 Pa gas pressure, $Ar/CF_4 = 100/100$ sccm gas flow, 500 W ICP source power, and 25 W RF bias power at 2 MHz.

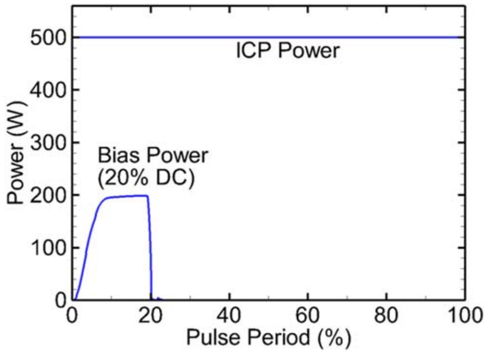

Figure 5. RF bias power waveform for bias-pulsed, 20% duty cycle Si etch process. Other operating conditions are 2 Pa gas pressure, 500 W ICP source power, and $HBr/Cl_2 = 200/100$ sccm gas flow.

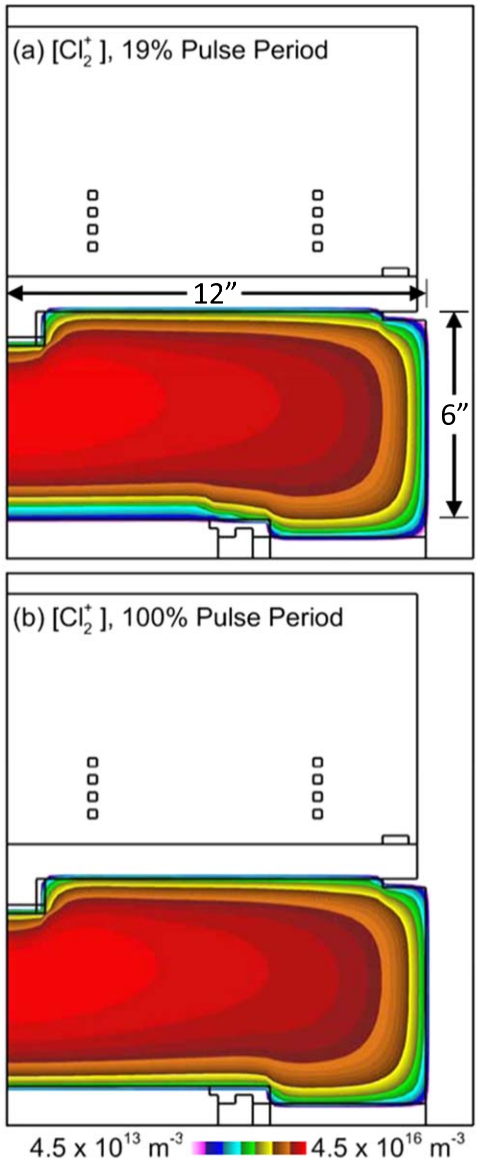

Figure 6. Cl_2^+ ion density for bias-pulsed, 20% duty cycle Si etch process: (a) right before the RF bias power is ramped down ('on') and (b) at the end of bias pulse ('off'). Other operating conditions are 2 Pa gas pressure, 500 W ICP source power, and $HBr/Cl_2 = 200/100$ sccm gas flow. During the 'on' phase, the RF bias power expands the sheath and reduces plasma density above the electrode.

etch rate/cycle at the top of the mask, the trench widths (CD) 20 nm from the mask—Si interface and CD approximately 50 nm from the bottom of the feature as a function of the number of cycles. The etch rates and CDs in the plots are averages of measurements at 12 locations. The mask erosion rate does not change during the etch process because the ion and neutral fluxes are invariant of time on the flat mask surface. The Si etch rate at the trench bottom however decreases as we etch deeper into the feature. This slowing of etch rate is due to the shadowing of neutral etchants (Cl, Br) within the HAR features, which reduces the etchant flux the deeper we dig. Focusing on CD at the top of the Si trenches, this CD increases slightly with number of cycles, and the top of the lines opens up during the etch process. Based on the results in figure 9, one can attribute this CD widening to mask erosion. Since the mask sidewalls are tapered, as the mask etches, the mask opening widens at the Si—mask interface. The CD near the feature bottom however indicates that the Si sidewalls are tapering inwards as we proceed through the etch process. One can attribute this to the oxidation step, which protects the Si sidewalls against etching, and shadowing at the feature corners. The role of oxidation will become clearer in subsequent discussion.

We next examine the effect of DC during bias-pulsed Si etch step. The RF bias power response is summarized in figure 13. All conditions other than the DC for RF bias power pulse are similar to the baseline. At smaller DCs (5%, 10%), the conservative ramping scheme does not allow the power to reach its prescribed peak value. At 15% and above, variations in DC simply extend the amount of time the RF bias is at full power before seeing the same rapid ramp down. As with the earlier analysis of the baseline 20% DC process, varying the bias pulse duration has little impact on the bulk plasma quantities but significant impact on the ion energies and fluxes. Ion energies at 10%, 20%, and 30% DC are examined in figures 14(a)–(c), respectively. For 10% DC, we again see lower energies during the ramp up (2%, 4%) and down (10%) periods. The equivalent portions of the ramps up and down

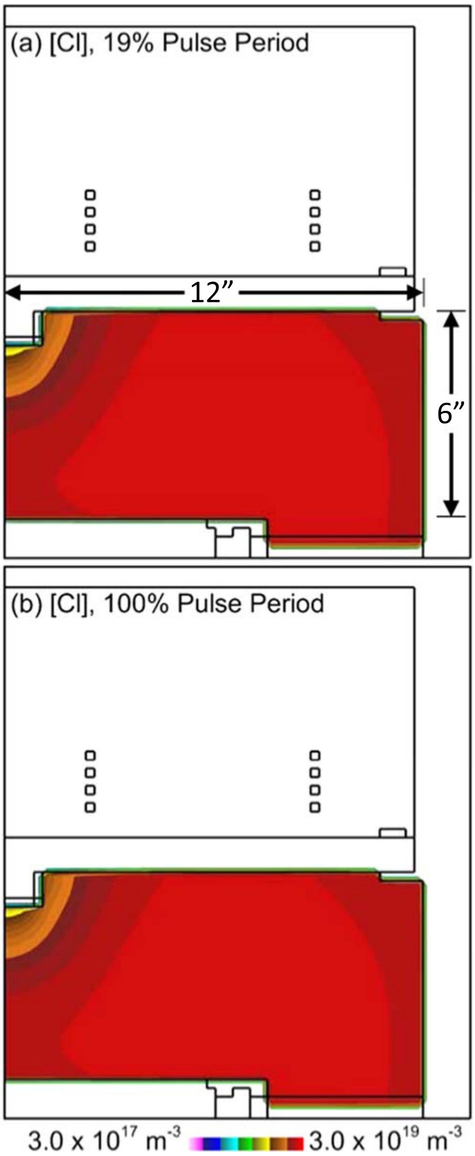

Figure 7. Cl radical density for bias-pulsed, 20% duty cycle Si etch process: (a) right before the RF bias power is ramped down ('on') and (b) at the end of bias pulse ('off'). Other operating conditions are 2 Pa gas pressure, 500 W ICP source power, and $HBr/Cl_2 = 200/100$ sccm gas flow.

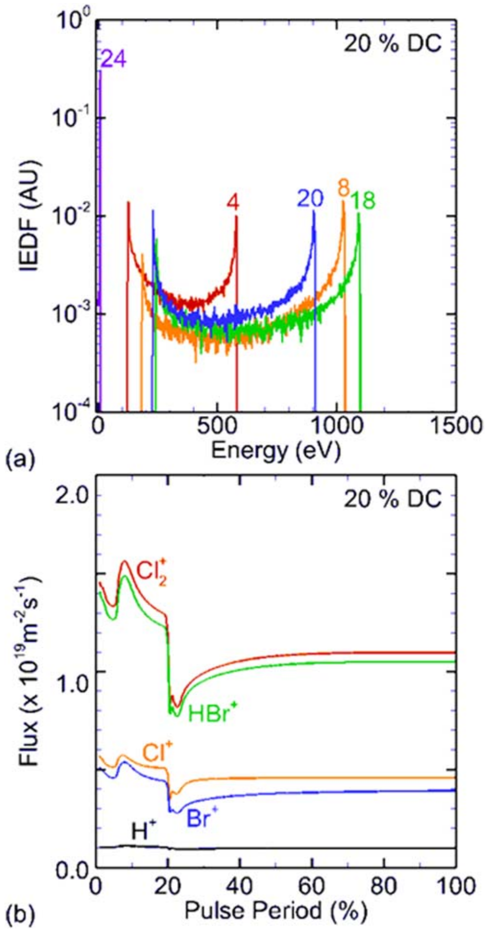

Figure 8. (a) Cl_2^+ ion energy distribution functions at different stages of the bias-pulsed, 20% duty cycle Si etch process. Number labels indicate percentage of pulse period at which the snapshot was taken. (b) Ion fluxes during the pulse for the bias-pulsed, 20% duty cycle Si etch process. Other operating conditions are 2 Pa gas pressure, 500 W ICP source power, $HBr/Cl_2 = 200/100$ sccm gas flow, and 200 W peak RF bias power.

for 20% and 30% DC are nearly identical. For the peak ion energy, however, the 10% DC is slightly less than that which is obtained at the higher DCs, as the bias power still has not reached its peak, an effect that would be even more pronounced at 5% DC.

Ion fluxes for the different bias DCs are given in figure 15. The increase in ion flux at the start of the bias pulse is essentially the same in each case. Then there is a similar decay profile until the RF bias is turned off, followed by a precipitous drop before recovering to the steady-state, source-only level.

It can be expected that the etch rates decrease as we decrease the DC due to less time with energetic ions. To examine the effect of DC during bias pulsing on the etch process, we compare the results at an approximate etch depth of 400 nm. The effect of DC during bias-pulsed Si etch step on *xz* profile is shown in figure 16. We have also shown the number of cycles needed to get to this depth for all DCs, which decreases with increasing DC. One can notice in figure 16 that slightly more mask remains after etching to the same Si etch depth when the DC is higher (40.42 nm at 10% DC versus 45.05 nm at 30% DC). In addition, the lines are more vertical at higher DC (slope is 0.83° from normal for 10% DC versus 0.68° at 30% DC). Since these changes are subtle and might be difficult to discern in figure 16, we next quantitatively examine the effect of DC during bias-pulsed Si etch step on etching characteristics. For quantitative analysis, we measured the etch depth at 12 locations at the trench bottom, at 12 locations at the top of the mask, and trench width (CD) at 12 locations. These measurements have been averaged and plotted in figure 17. Figure 17(a) includes the effect of DC on etch rate at Si bottom and at the top of the mask. Both etch rates increase almost linearly with the DC. It is important to point out that the etch rate does not become zero at zero DC due to etching of both Si and mask during the clean step, where ions have sufficient energy to etch these

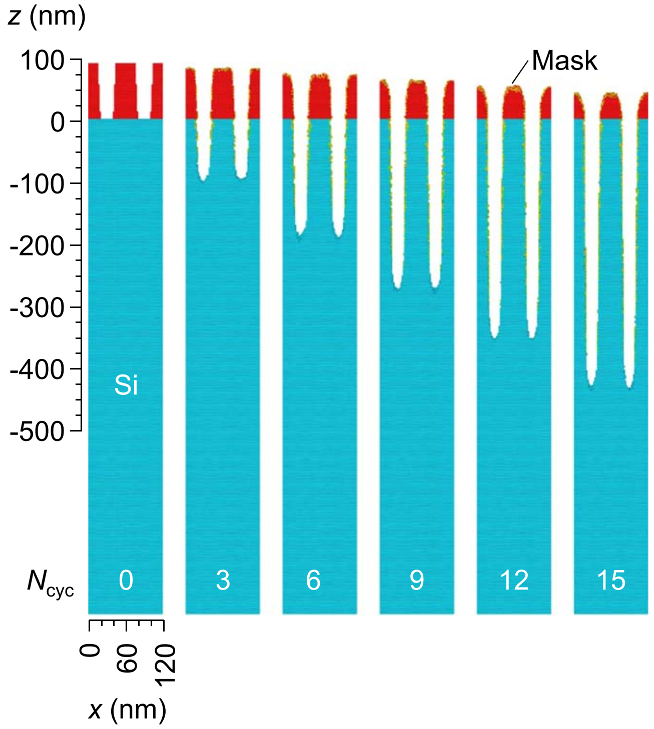

Figure 9. *xz* cross-section of the structure (as viewed from the $y < 0$ region) for the bias-pulsed, 20% duty cycle Si etch process. The cross-sections are plotted as a function of the number of cycles of the three-step etch sequence. During the Si etch step, operating conditions are 2 Pa gas pressure, 500 W ICP source power, $HBr/Cl_2 = 200/100$ sccm gas flow, and 200 W peak RF bias power.

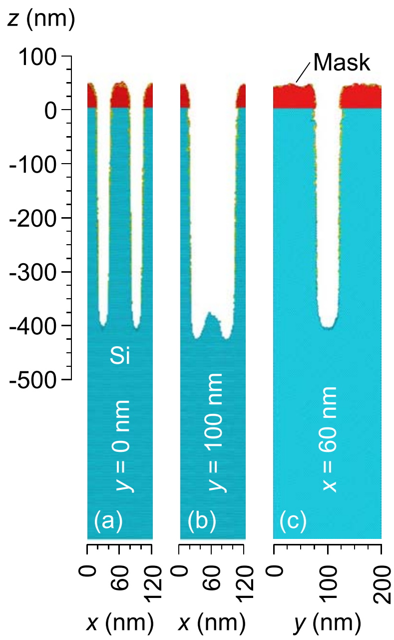

Figure 10. Different cross-sections of the three-dimensional structure after 15 cycles of etching: (a) *xz* profile viewed from the $y < 0$ region, (b) *xz* profile of a thin sliver near $y = 100$ nm, and (c) *yz* profile of a thin sliver near $x = 60$ nm. During the Si etch step, operating conditions are 2 Pa gas pressure, 500 W ICP source power, $HBr/Cl_2 = 200/100$ sccm gas flow, and 200 W peak RF bias power. The RF bias power is pulsed at 20% duty cycle.

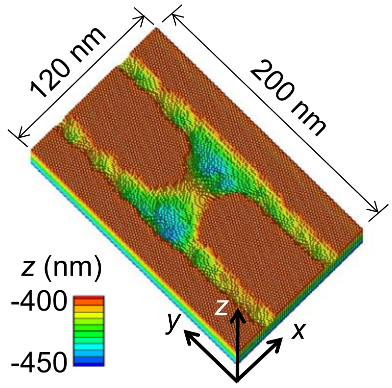

Figure 11. The three-dimensional structure viewed after 15 cycles of etching. To show the bottom surface profile, all material above $z = -400$ nm has been removed in this image. All material is Si and the color indicates the depth. During the Si etch step, operating conditions are 2 Pa gas pressure, 500 W ICP source power, $HBr/Cl_2 = 200/100$ sccm gas flow, and 200 W peak RF bias power. The RF bias power is pulsed at 20% duty cycle.

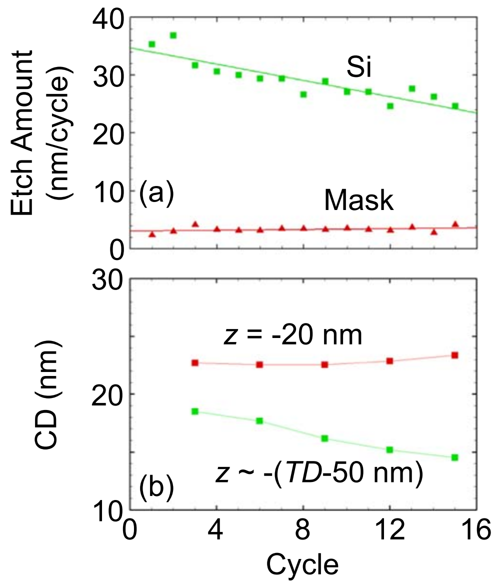

Figure 12. (a) Si and mask etch rate as a function of the number of etch cycles. (b) Critical dimension (CD) at two heights, (red) fixed position and (green) 50 nm beyond the trench depth (TD). During the Si etch step, operating conditions are 2 Pa gas pressure, 500 W ICP source power, $HBr/Cl_2 = 200/100$ sccm gas flow, and 200 W peak RF bias power. The RF bias power is pulsed at 20% duty cycle.

materials. We have plotted the ratio of Si and mask etch rate (i.e., etch selectivity) in figure 17(b) as a function of DC. Although there is some variation due to the statistical nature of our Monte Carlo feature scale simulation, etch selectivity increases with increasing DC, implying that relatively more mask etching occurs at lower DC. Detailed analysis of our results indicates that this decrease in selectivity at lower DC is due to the increase in the number of cycles, which increases the total duration of the clean process. The clean process has fluorocarbon species and ions with energy approaching 50 eV, so is well-suited for reactive ion etching of SiO_2-like materials. At these ion energies, one does not expect aggressive Si etch due to fluorocarbon polymerization.

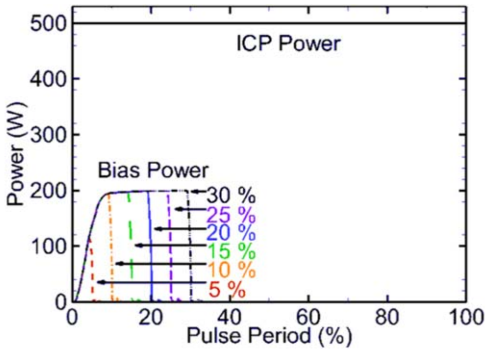

Figure 13. RF bias power waveforms for bias-pulsed Si etch processes. Number labels indicate duty cycle of RF bias pulse. Other operating conditions are 2 Pa gas pressure, 500 W ICP source power, $HBr/Cl_2 = 200/100$ sccm gas flow, and 200 W peak RF bias power.

Focusing on CDs in figure 17(c), we have plotted these near the Si—mask interface and close to the trench bottom. The CD increases both at the feature top and bottom with increasing DC, although more so at the feature bottom. This increase in line CD with increasing DC can be attributed to lower number of cycles needed to etch to the same depth, which reduces the total oxidation time. Oxidation helps protect the Si sidewall, so the sidewalls are more prone to reactive ion etch by off-normal ions during the main Si etch step when the DC is higher.

Another pulsing scheme of interest is synchronized pulsing of both the ICP source and RF bias powers where we control the phase between them. In figure 18, we show ICP source and RF bias powers for synchronized pulsing scheme with four different phases. Here, ICP source and RF bias powers are pulsed with 30% DC at 2 kHz. The RF power pulse leads the ICP source power pulse by 0° (in-phase), 90°, 180°, and 270° in the 4 cases considered. While pulsing the ICP source power can significantly change the bulk plasma during its off-phase, here we focus our analysis on the impact of this scheme on ion energies and fluxes. In figure 19, ion energies during different portions of the pulse are shown for the different bias phases. For the in-phase (0°) case, the ion energies at different sections of the pulse are similar to the bias-pulsed 30% DC case. There is a slight shift higher in energy for the in-phase pulse, however, as the smaller time-averaged source power leads to lower plasma densities. As a result, bias voltages shift higher to reach the desired power level. With changing phase, a similar dynamic tends to shift ion energies higher than the in-phase case. For the 90° bias-leading scenario, plasma density at the start of the bias pulse can be quite low, as the source has been off for 45% of the pulse before the bias comes on, forcing voltages higher. This phenomenon decreases with the 180° phase, where the source is only off for 20% of the cycle prior to the bias coming on. At 270° phase, there is 5% overlap between source and bias when the bias comes on, but still significantly higher ion energies are observed by the end of the pulse than for the in-phase case.

Ion fluxes for these schemes are illustrated in figure 20. In general, the ICP source power at the start of the pulse provides a burst of ion flux, and the applied RF bias either enhances this burst or provides its own secondary flux depending on phase. For the in-phase 0° scenario, we observe a high, sustained level of ion flux when both powers are on, followed by a sharp drop for the duration of the off-phase. For the 90° and 180° bias-leading cases, the source and bias

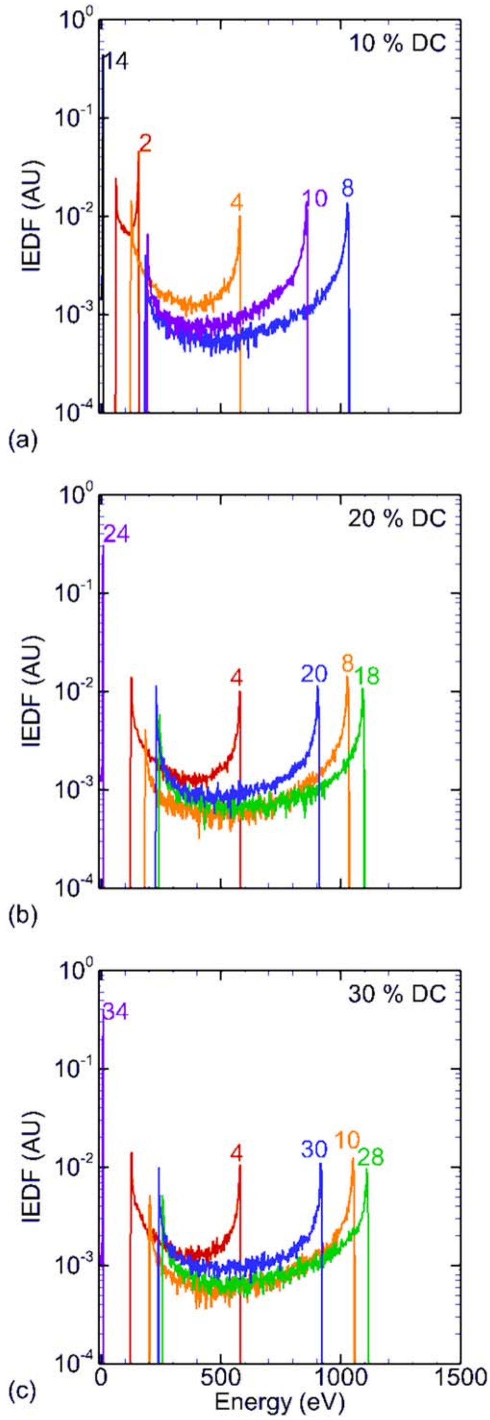

Figure 14. Cl_2^+ ion energy distribution functions for bias-pulsed Si etch processes. (a) 10% duty cycle, (b) 20% duty cycle, and (c) 30% duty cycle. Number labels indicate percentage of pulse period at which the snapshot was taken. Other operating conditions are 2 Pa gas pressure, 500 W ICP source power, $HBr/Cl_2 = 200/100$ sccm gas flow, and 200 W peak RF bias power.

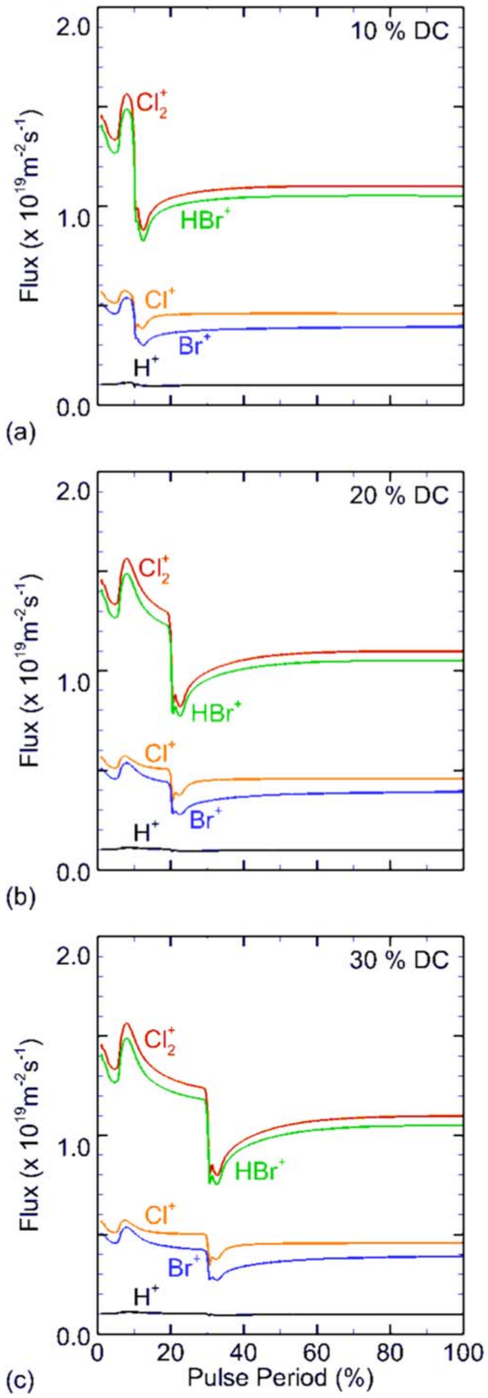

Figure 15. Ion fluxes during the pulse for bias-pulsed Si etch processes. (a) 10% duty cycle, (b) 20% duty cycle, and (c) 30% duty cycle. Other operating conditions are 2 Pa gas pressure, 500 W ICP source power, $HBr/Cl_2 = 200/100$ sccm gas flows, and 200 W peak RF bias power.

power-driven fluxes are nearly completely distinct. By the time the bias power is on, the source plasma has largely extinguished. For the 90° lead, the small overlap at the end of the bias pulse perturbs but does appear to enhance the ion flux from the source pulse. The opposite is true for the overlap of the end of the source pulse and start of the bias pulse for the 270° bias lead. Here, the ion flux from the source-only portion is increased to an even higher level when the bias turns on.

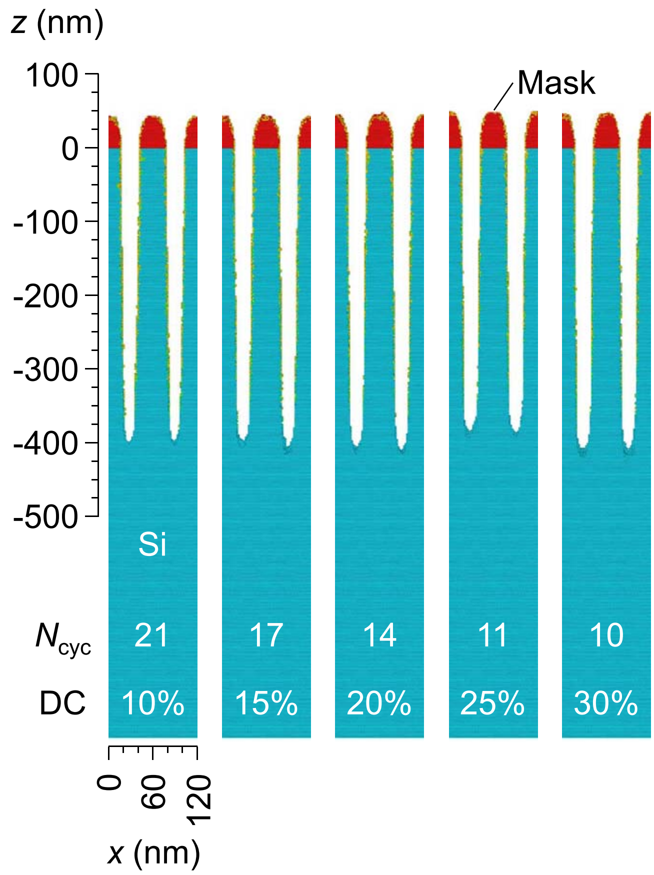

Figure 16. xz cross-section of the structure (as viewed from the $y < 0$ region) as a function of duty cycle during the bias-pulsed Si etch process. The number of cycles of the three-step etch sequence needed to etch to a depth of ~400 nm is also shown. During the Si etch step, operating conditions are 2 Pa gas pressure, 500 W ICP source power, $HBr/Cl_2 = 200/100$ sccm gas flow, and 200 W peak RF bias power. RF bias power is pulsed.

For all of these profiles, however, it should be noted that the important quantity is not the raw ion flux, but the energetic ion flux. For the 90° and 180° bias-leading phases, the ion flux arising from the source power is largely going towards low energy species.

Focusing next on feature scale results, in figure 21, we have shown the xz view of the structure as a function of phase difference between ICP source and RF bias powers. Results have been plotted after one has etched to a depth of approximately 400 nm. We have also shown the number of cycles needed to get to this depth. The etch process is fastest when both the ICP source and RF bias powers are pulsed in phase (0°). The remaining mask is also thickest for this condition, and the trenches are most open (sidewalls are sloped at 0.49° from normal at 0° phase lag and 0.71° at 90° phase lag).

To quantitatively examine the effect of phase shift on etching characteristics, we have plotted etch rates, etch selectivity and trench CDs in figure 22. All results are averages from 12 locations. Please note that results for phase shift of 0° have been repeated at 360° to emphasize the cyclic nature of phase shift. Figure 22(a) includes the effect of phase shift on etch rate at Si trench bottom and at the top of the

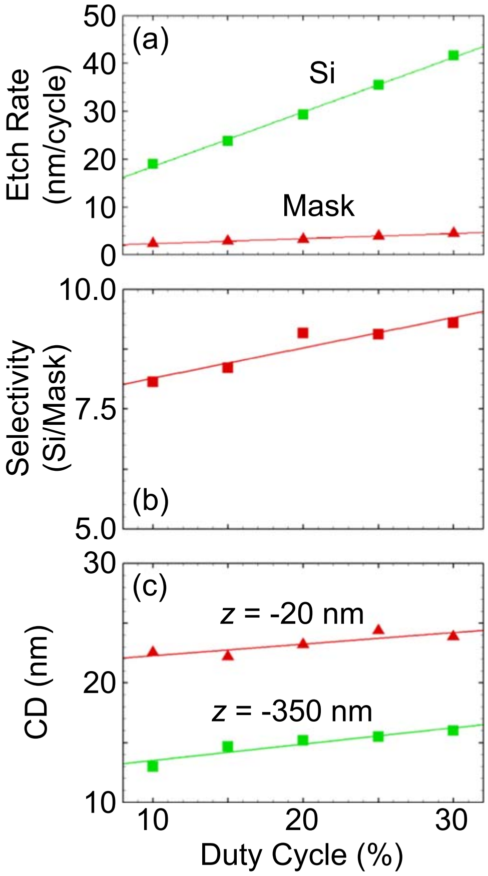

Figure 17. The effect of duty cycle during bias pulsing on (a) the Si and mask etch rates, (b) the selectivity (Si/Mask), and (c) trench width at two heights. During the Si etch step, operating conditions are 2 Pa gas pressure, 500 W ICP source power, $HBr/Cl_2 = 200/100$ sccm gas flow, and 200 W peak RF bias power.

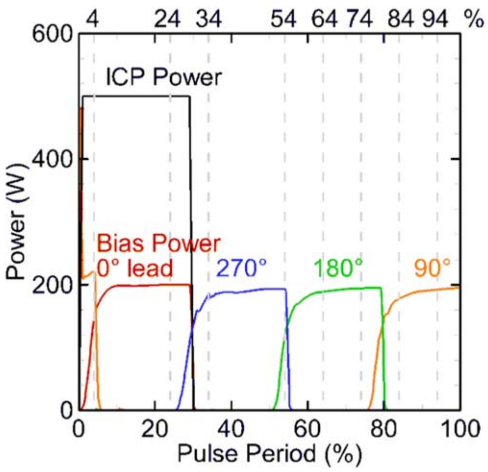

Figure 18. ICP source and RF bias power waveforms for synchronized pulsed Si etch processes. Number labels indicate phase angle by which the RF bias pulse leads the ICP source pulse. Both source and bias powers are pulsed with 30% duty cycle. Other operating conditions are 2 Pa gas pressure, 500 W peak ICP source power, $HBr/Cl_2 = 200/100$ sccm gas flow, and 200 W peak RF bias power.

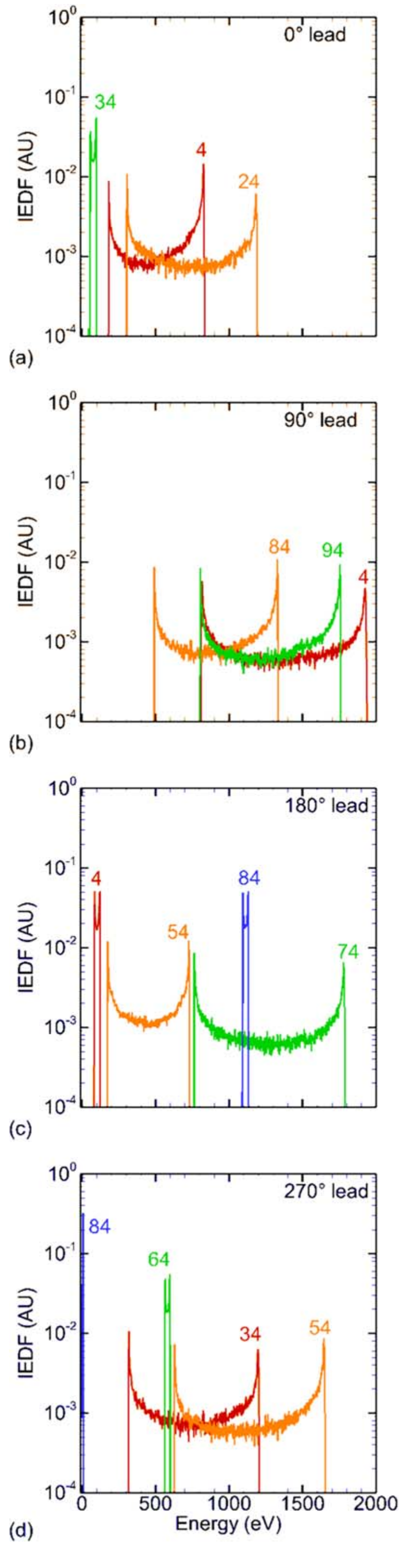

Figure 19. Cl_2^+ ion energy distribution functions for synchronized pulsed Si etch processes. (a) 0° bias lead, (b) 90° bias lead, (c) 180° bias lead, and (d) 270° bias lead. Number labels indicate percentage of pulse period at which the snapshot was taken. Other operating conditions are 2 Pa gas pressure, 500 W peak ICP source power, $HBr/Cl_2 = 200/100$ sccm gas flow, and 200 W peak RF bias power. Both ICP source and RF bias powers are pulsed with 30% duty cycle.

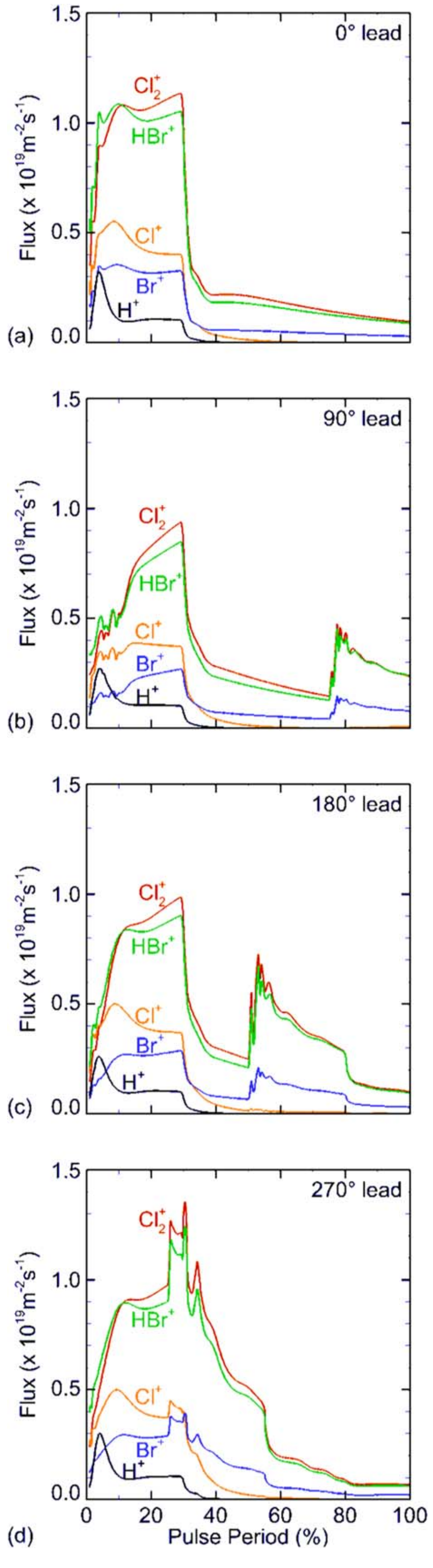

Figure 20. Ion fluxes during the pulse for synchronized pulsed Si etch processes. (a) 0° bias lead, (b) 90° bias lead, (c) 180° bias lead, and (d) 270° bias lead. Other operating conditions are 2 Pa gas pressure, 500 W peak ICP source power, $HBr/Cl_2 = 200/100$ sccm gas flow, and 200 W peak RF bias power. Both ICP source and RF bias powers are pulsed with 30% duty cycle.

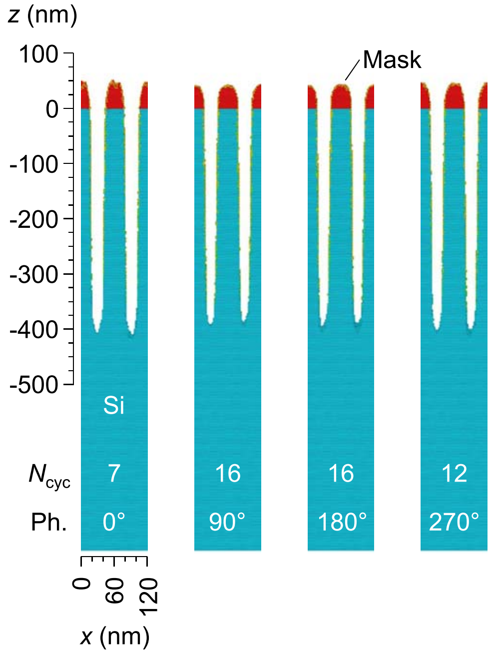

Figure 21. xz cross-section of the structure (as viewed from the $y < 0$ region) as a function of phase angle during synchronized pulsed Si etch processes. The number of cycles of the three-step etch sequence needed to etch to a depth of ~400 nm is also shown. During the Si etch step, operating conditions are 2 Pa gas pressure, 500 W peak ICP source power, $HBr/Cl_2 = 200/100$ sccm gas flow, and 200 W peak RF bias power. Both ICP source and RF bias powers are pulsed with 30% duty cycle.

mask. Both etch rates are highest at a phase shift of 0° and lowest between 90° and 180°. Si is mainly etched through reactive ion etching by Cl and Br along with energetic ions. Neutral radical fluxes do not change appreciably at 2 kHz pulsing frequency. One would therefore expect the Si etch rate to be highest when both the ion flux and ion energy are high. Based on results in figure 20, the ion flux is highest when the source is on. Similarly, as shown in figure 19, the ions are most energetic when RF bias power is turned on. High ion flux and high ion energy clearly coincide when bias and source are pulsed in phase (0°, 360°). Decreasing the phase from 360° to 270°, the RF bias is only turned on towards the end (5% of pulse period) of the source-on pulse. Therefore, for most of the time with high ion flux, the ion energy is negligible. The ion flux decreases rapidly during most of the bias-on, high ion energy phase, so etch rate for both materials is lower at 270° compared to 360°. The high ion flux (source-on) and high ion energy (bias-on) periods are separate for 180° phase shift, so Si and mask etch rates are even lower. We have plotted the Si/mask etch selectivity in figure 22(b) as a function of phase shift. Etch selectivity is highest when phase shift is 0° and lowest between 90° and 180°. Similar to the impact of lowering DC with bias pulsing, asynchronous (i.e., not 0° phase shift) use of source and bias pulsing ultimately requires a higher number of cycles to reach the same etch depth. The increased use of the less selective clean process again reduces overall selectivity. Focusing on CDs in figure 22(c), one finds that the CD at both the top and bottom of the features is largest at phase shift of 0° and lowest

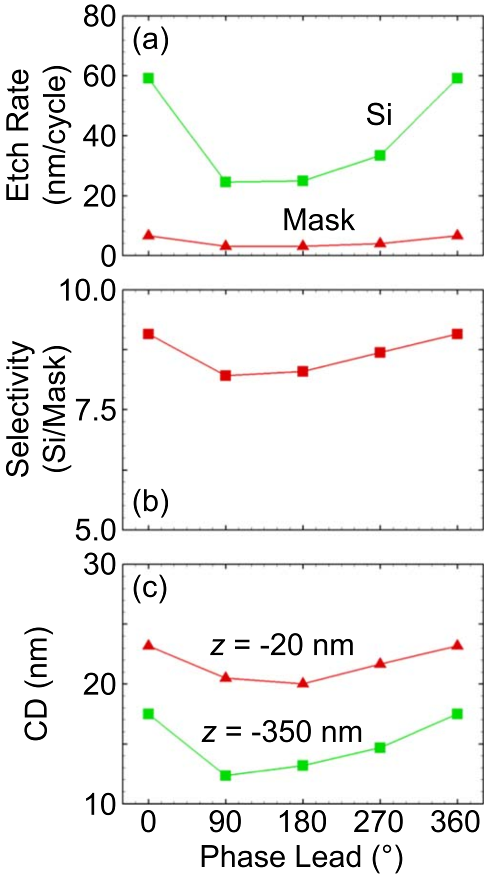

Figure 22. The effect of phase angle during synchronized pulsed Si etch processes on (a) the Si and mask etch rates, (b) the selectivity (Si/Mask), and (c) trench width at two heights. During the Si etch step, operating conditions are 2 Pa gas pressure, 500 W peak ICP source power, $HBr/Cl_2 = 200/100$ sccm gas flow, and 200 W peak RF bias power. Both ICP source and RF bias powers are pulsed with 30% duty cycle.

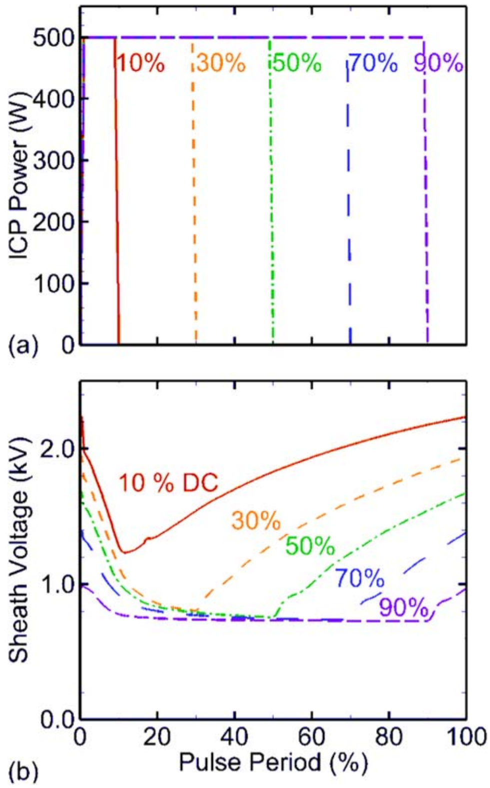

Figure 23. (a) ICP source power waveforms for source-pulsed Si etch process. (b) Average sheath voltage during the pulse for source-pulsed Si etch process. Other operating conditions are 2 Pa gas pressure, 500 W peak ICP source power, $HBr/Cl_2 = 200/100$ sccm gas flow, and 200 W RF bias power.

between 90° and 180°. The dependence of trench CD on phase shift can be directly linked to the number of cycles needed to etch to the same depth. Oxidation helps protect the Si sidewall, so the sidewalls are more prone to reactive ion etch by off-normal ions with less oxidation time.

A final power modulation considered is that of pulsing the ICP source power with leaving on the RF bias power. In figure 23(a), several ICP source power DCs are illustrated ranging from 10% to 90%, and figure 23(b) shows the corresponding observed sheath voltage during the pulse. At 90% DC, the source is nearly in CW mode, and the sheath has only a slight rise during the final 10% of the pulse before decaying back to the CW level when the ICP source power is turned back on. This dynamic continues in similar fashion as the source DC is decreased, with ever-increasing peak sheath voltages returning to near CW levels up to around 30% DC. Lowering the DC further does not allow the source power to fully develop a CW-like plasma, and sheath voltages trend even higher and no longer decrease to the CW level.

As expected from the earlier results, ion fluxes are a strong function of the source DC. These are plotted in figure 24 for three DCs, and they show different behaviors linked to the different effective ICP source power levels. At low DC (10%), there is a relatively low-level spike in ion flux as the source turns on, which then slowly decays. At moderate DC (50%), a large ion flux builds up that does not quite reach steady-state before the source turns off and rapidly decays. At high DC (90%), the ion flux reaches a steady-state level relatively soon after the source turns on, then owing to the small amount of time the source is off, suffers only a small decay in flux at the end of the pulse.

Ion energies follow somewhat the inverse of the ion flux results, as shown in figure 25. At low DC, ion energies trend higher as the RF bias voltage must be increased to compensate for the lower plasma densities. As the plasma density steadily increases for the 50% and 90% DC cases, the sheath voltages decrease, resulting in lower energies.

Examining the feature scale results next, we have shown the structure after one has etched to a depth close to 400 nm in figure 26 as a function of DC during source pulsing. We have also shown the number of cycles needed to get to this depth for all phases. With the bias power on continuously, Si etches at a fast rate. Therefore, fewer cycles are needed to reach 400 nm than the other pulsing modes. Due to high etch rate per cycle, it has been difficult to compare the results at the same depth. This is especially true for DC $>$ 50%. One can observe that the mask has significantly eroded for 10% DC and mask gets better retained as we increase the source power DC. The trenches are also thinner with tapered sidewalls at lower DC.

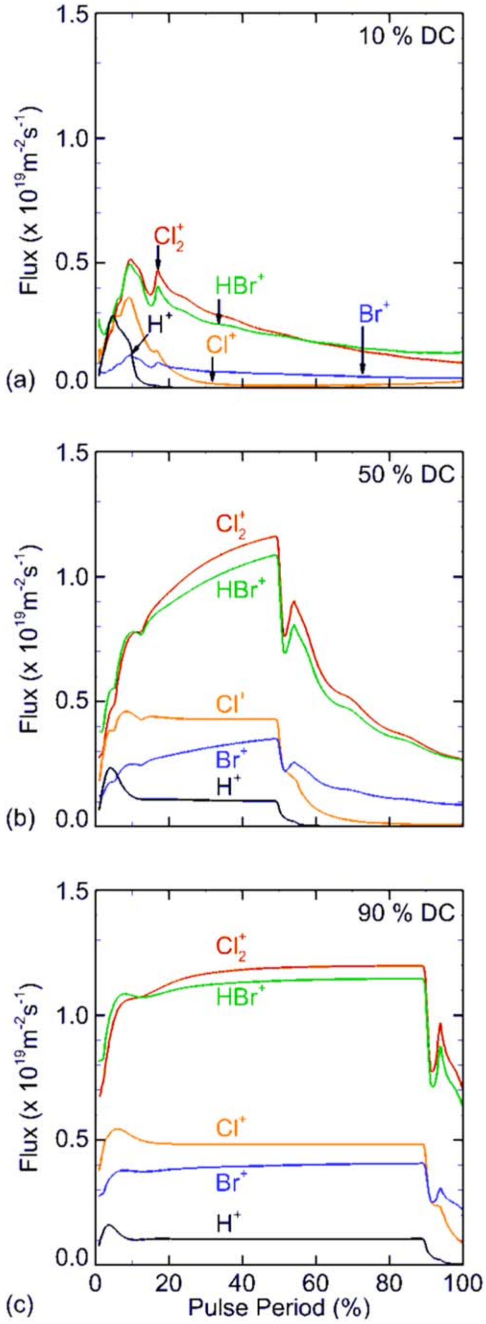

Figure 24. Ion fluxes during the pulse for source-pulsed Si etch processes: (a) 10% duty cycle, (b) 50% duty cycle, and (c) 90% duty cycle. Other operating conditions are 2 Pa gas pressure, 500 W peak ICP source power, $HBr/Cl_2 = 200/100$ sccm gas flow, and 200 W RF bias power.

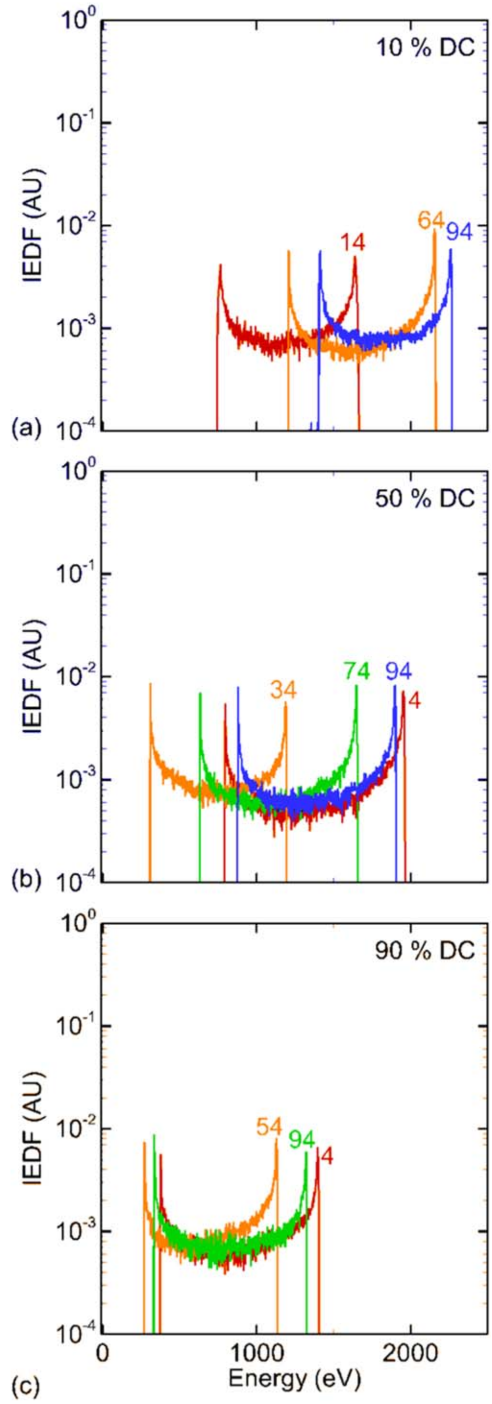

Figure 25. Cl_2^+ ion energy distribution functions for source-pulsed Si etch processes: (a) 10% duty cycle, (b) 50% duty cycle, and (c) 90% duty cycle. Number labels indicate percentage of pulse at which snapshot was taken. Other operating conditions are 2 Pa gas pressure, 500 W peak ICP source power, $HBr/Cl_2 = 200/100$ sccm gas flow, and 200 W RF bias power.

To quantitatively examine the effect of DC during source pulsing on etching characteristics, we have plotted etch rates, etch selectivity and trench CDs in figure 27. Figure 27(a) includes the effect of source pulsing DC on etch rate at Si trench bottom and at the top of the mask. Both etch rates increase monotonically with increasing DC. The Si etch depth slope changes beyond 50% DC, which is likely due to measurement at different etch depths. As RF bias power is continuously on, both materials are etched always. However, when the source is on, ion flux is significantly higher and it decreases exponentially during the source off phase. One can observe from the results in figure 24 that cycle-averaged ion flux increases monotonically with DC, which results in higher etch rate at larger DC. We have plotted the Si/mask etch selectivity in figure 27(b) as a function of source pulsing DC. The etch selectivity increases monotonically with DC. Detailed analysis of our results shows that lower selectivity at

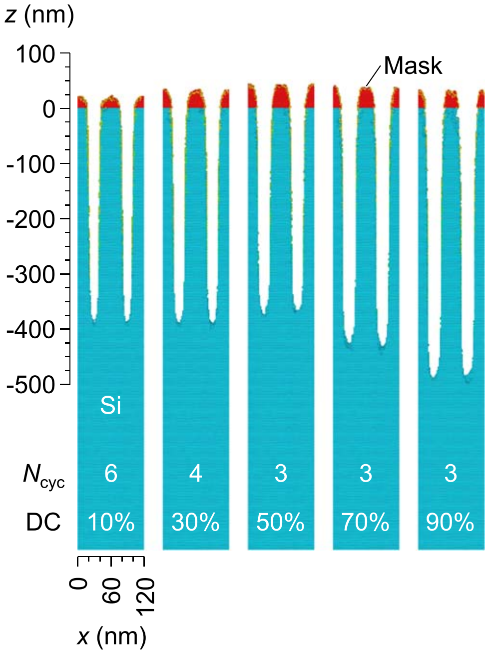

Figure 26. xz cross-section of the structure (as viewed from the $y < 0$ region) as a function of duty cycle during source-pulsed Si etch processes. The number of cycles of the three-step etch sequence needed to etch to a depth of ~400 nm is also shown. During the Si etch step, operating conditions are 2 Pa gas pressure, 500 W peak ICP source power, $HBr/Cl_2 = 200/100$ sccm gas flow, and 200 W RF bias power.

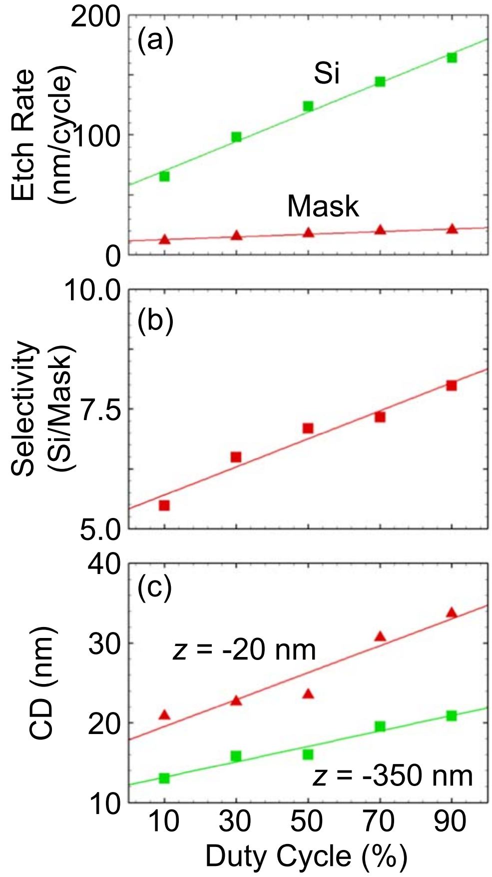

Figure 27. The effect of duty cycle during source-pulsed Si etch processes on (a) the Si and mask etch rates, (b) the selectivity (Si/Mask), and (c) trench width at two heights. During the Si etch step, operating conditions are 2 Pa gas pressure, 500 W peak ICP source power, $HBr/Cl_2 = 200/100$ sccm gas flow, and 200 W RF bias power.

smaller DC is due to lower ion flux and higher ion energy at lower DC. The relative importance of sputtering in Si removal gets enhanced in this regime, and sputtering is a much less selective etch process. Focusing on CDs in figure 22(c), one can observe that the CD at both the top and bottom of the Si trenches increases with source power DC. The slopes are different below and above 50% DC, which are likely because the measurement have been made at different depths. The dependence of trench CD on phase difference can be directly linked to the number of cycles needed to etch to the same depth. Oxidation helps protect the Si sidewall, so the sidewalls are more prone to reactive ion etch by off-normal ions when the total oxidation time is reduced.

4. Conclusions

A coupled 2D plasma—3D feature scale model has been utilized to investigate HAR Si etching using a multi-step cyclic etch process in an ICP reactor. Both the ICP source and RF bias powers are pulsed during the main Si etch step, and etching results are compared for several pulsing modes. When only the RF bias power is pulsed, bulk plasma characteristics do not change significantly during the pulse. The RF bias however influences the sheath above the wafer, significantly modulating both the ion flux at the wafer and IEAD. Feature scale modeling shows that the mask erodes considerably during the etch process due to high ion energy during the main Si etch step, which leads to widening of the CD near the Si—mask interface. Si sidewalls are protected using a separate oxidation process in the etch sequence, and this oxidation results in tapered Si sidewalls. The bottom Si surface is not planar, with higher etch rate where the surface has more visibility to the plasma.

During bias-pulsed Si main step, DC has significant influence on the ions and therefore the etch process. Both Si and the mask etch faster at higher DC due to more time with energetic ions. Consequently, if one etches to the same depth, the total time for both oxidation and clean are reduced. Clean time reduction helps improve mask selectivity while oxidation time reduction leads to more open trenches with larger CDs. Synchronized pulsing of both the ICP source and RF bias powers allows one to better control the IEAD and ion flux. When both the source and bias powers are pulsed in phase (0°), the time of high ion flux and high ion energy coincide. Therefore, Si and mask etch fastest at 0° phase difference, along with highest selectivity and largest CDs for reasons explained above. We also examined source pulsing where RF bias power is kept continuously on. In this mode, the ion energy can be increased considerably at low source pulsing DCs. As RF bias power is continuously on during source-pulsing, Si and the mask etched at rates much higher than in other pulsing modes. The high ion energy, however, had the deleterious effect of shifting the Si etch process more towards sputtering relative to reactive ion etch, which decreased mask selectivity considerably.

The ability to pulse both the ICP source and RF bias allows one to modulate ion energy and flux over a wide range. This capability is critical for fabrication of sub-10 nm microelectronic technologies.

HAR Si etching using multi-step pulsed plasmas is an expansive topic and we only discussed the fundamental etch characteristics of several pulsing modes in this paper. Other important details such as uniformity of the etching profiles and etch profile near the wafer edge are captured by our model. We hope to cover these aspects of the etch process in a subsequent publication.

Acknowledgments

The authors would like to thank M Li, C Chen, K Muthukrishnan, M Kiehlbauch, A Schrinsky, M Koltonski, A Wilson, C Huffman, K Tokashiki, W Chang, X Yang and I MacKinnon for useful technical discussions and support.

ORCID iDs

S Rauf https://orcid.org/0000-0001-5689-6115
S C Pandey https://orcid.org/0000-0002-2629-0822

References

[1] Donnelly V M and Kornblit A 2013 *J. Vac. Sci. Technol.* A **31** 050825
[2] Shiozawa K *et al* 1999 *Japan. J. Appl. Phys.* **38** L234
[3] Wu B, Kumar A and Pamarthy S 2010 *J. Appl. Phys.* **108** 051101
[4] Cho E *et al* 2008 Study of shallow trench isolation dry etching process using oxide hard mask and KrF photo-resist in 90 nm stand-alone flash device *Proc. Adv. Resist Mater. Process. Technol.* vol 25, p 69233
[5] Choi S and Hong S J 2015 *Trans. Electr. Electron. Mater.* **16** 312
[6] Banna S, Agarwal A, Cunge G, Darnon M, Pargon E and Joubert O 2012 *J. Vac. Sci. Technol.* A **30** 040801
[7] Tokashiki K *et al* 2009 *Japan. J. Appl. Phys.* **48** 08HD01
[8] Samukawa S and Mieno T 1996 *Plasma Sources Sci. Technol.* **5** 132
[9] Agarwal A, Stout P J, Banna S, Rauf S, Tokashiki K, Lee J-Y and Collins K 2009 *J. Appl. Phys.* **106** 103305
[10] Laermer F and Urban A 2003 *Microelectron. Eng.* **67–68** 349
[11] Dussart R *et al* 2004 *J. Micromech. Microeng.* **14** 190
[12] Blauw M A, van der Drift E, Marcos G and Rhallabi A 2003 *J. Appl. Phys.* **94** 6311
[13] Azimi S, Mohajerzadeh S, Amini A, Vali A and Mehran M 2010 *Trans. F. Nanotechnol.* **17** 113
[14] Stout P J, Rauf S, Nagy A and Ventzek P L G 2006 *J. Vac. Sci. Technol.* B **24** 1344
[15] Stout P J and Zhang D 2002 *IEEE Trans. Plasma Sci.* **30** 116
[16] Rauf S, Dauksher W J, Clemens S B and Smith K H 2002 *J. Vac. Sci. Technol.* A **20** 1177
[17] Hoang J, Hsu C C and Chang J P 2008 *J. Vac. Sci. Technol.* B **26** 1911
[18] Kenney J, Rauf S and Collins K 2009 *J. Appl. Phys.* **106** 103302
[19] Rauf S, Kenney J and Collins K 2009 *J. Appl. Phys.* **105** 103301
[20] Ventzek P L G, Hoekstra R J and Kushner M J 1994 *J. Vac. Sci. Technol.* B **12** 461
[21] Stout P J, Rauf S, Peters R D and Ventzek P L G 2006 *J. Vac. Sci. Technol.* B **24** 1810
[22] Hoekstra R J, Grapperhaus M J and Kushner M J 1997 *J. Vac. Sci. Technol.* A **15** 1913
[23] Chang J P and Sawin H H 1997 *J. Vac. Sci. Technol.* A **15** 610
[24] Standaert T E F M, Schaepkens M, Rueger N R, Sebel P G M, Oehrlein G S and Cook J M 1998 *J. Vac. Sci. Technol.* A **16** 239
[25] Schaepkens M, Standaert T E F M, Rueger N R, Sebel P G M, Oehrlein G S and Cook J M 1999 *J. Vac. Sci. Technol.* A **17** 26
[26] Doering R and Nishi Y (ed) 2008 *Handbook of Semiconductor Manufacturing Technology* 2nd edn (Boca Raton, FL: CRC Press) ch 13
[27] Shimmura T, Soda S, Samukawa S, Koyanagi M and Hane K 2002 *J. Vac. Sci. Technol.* B **20** 2346
[28] Rauf S and Kushner M J 1997 *J. Appl. Phys.* **82** 2805
[29] Gul B, Ahmad I, Zia G and Rehman A U 2016 *Phys. Plasmas* **23** 093508